

# Particle injection and reacceleration in clusters of galaxies and the EUV excess: the case of Coma

G. Brunetti <sup>a,1</sup>, G. Setti <sup>a,2</sup>, L. Feretti <sup>b,3</sup>, G. Giovannini <sup>c,4</sup>

<sup>a</sup> *Dipartimento di Astronomia, Università di Bologna, via Ranzani 1, I-40127 Bologna, Italy. Istituto di Radioastronomia del CNR, via Gobetti 101, I-40129 Bologna, Italy.*

<sup>b</sup> *Istituto di Radioastronomia del CNR, via Gobetti 101, I-40129 Bologna, Italy.*

<sup>c</sup> *Dipartimento di Fisica, Università di Bologna, via Bertini-Pichat 6/2, I-40127 Bologna, Italy. Istituto di Radioastronomia del CNR, via Gobetti 101, I-40129 Bologna, Italy.*

---

## Abstract

We calculate the energy distribution of the relativistic particles injected in the ICM during a phase of reacceleration of the relativistic particles in the cluster volume. We apply our results to the case of the Coma cluster in which recent merging activity and the presence of the radio halo may suggest that reacceleration processes are efficient. We find that the electron population injected in the central part of the cluster by the head-tail radio galaxy NGC 4869 may account for a large fraction, if not all, of the detected EUV excess via inverse Compton scattering of the cosmic microwave background (CMB) photons.

If radio haloes are powered by reacceleration mechanisms active in the cluster volume, moderate non-thermal EUV excesses (of order of  $\sim 1 - 5 \cdot 10^{42} \text{erg s}^{-1}$ ) should be a common feature of clusters containing powerful head-tail radio galaxies and/or AGNs.

*PACS:* 95.30.Cq; 95.30.Gv; 98.54.Gr; 98.65.Cw; 98.65.Hb

*Key words:* acceleration of particles – radiation mechanisms: non-thermal – galaxies: active - galaxies: clusters: general - galaxies: clusters: individual: Coma - ultraviolet: general

---

## 1 Introduction

Observations of a few galaxy clusters with the *Extreme Ultraviolet Explorer* have revealed extreme ultraviolet emission (EUV) in excess of that expected by extrapolating downward the thermal X-ray spectrum (Lieu et al. 1996a,b; Bowyer, Lampton and Lieu 1996; Mittaz, Lieu and Lockman 1998). The EUV excess has been claimed by these authors as a new feature of clusters of galaxies with important physical implications.

The suggestion that spurious EUV excesses may derive by underestimating the line-of-sight Galactic absorption (Arabadjis & Bregman 1999) has been excluded by further EUV investigations (Bowyer, Berghöfer and Korpela 1999). These authors have also pointed out that the measured EUVs are strongly influenced by the variation of the telescope sensitivity over the field of view. By making use of the appropriate corrections, EUV extended excess was confirmed in the case of Coma (Bowyer et al. 1999) and Virgo (Berghöfer, Bowyer and Korpela 2000), whereas no evidence of extended EUV excess was found in A1795 and A2199 (Bowyer et al. 1999). The presence of EUV excess in the latter two clusters is, however, still debated (Bonamente, Lieu and Mittaz 2000; Lieu, Bonamente and Mittaz 2000).

The EUV excess may be interpreted as due to a relatively cool ( $\sim 10^6$  K) emitting gas (e.g. Lieu et al. 1996a), but, at these temperatures the gas cooling is particularly efficient, so that a non-thermal interpretation is usually favoured with respect to the thermal scenario (Hwang 1997; Ensslin & Biermann 1998; Bowyer & Berghöfer 1998; Sarazin & Lieu; Lieu et al. 1999). Indeed, synchrotron emission in the radio band and inverse Compton (IC) emission in the EUV and hard X-rays are expected from clusters of galaxies in the framework of continuous injection of relativistic electrons (Sarazin 1999; Völk & Atoyan 1999) and of a *two phase* model invoking reacceleration of previously injected relic particles (Brunetti et al. 2000).

Due to the large amount of data the Coma cluster represents the best case to compare model predictions with observations. Since the EUV profile is narrower than the radio one, it cannot be accounted for by IC emission of the low energy halo electrons with the CMB photons (Bowyer & Berghöfer 1998). Thus, alternative scenarios have been explored.

Ensslin et al. (1999) have calculated that anisotropic IC scattering of the optical photons (from the central galaxies in the cluster) by an assumed ad

---

<sup>1</sup> gbrunetti@astbo1.bo.cnr.it

<sup>2</sup> setti@astbo1.bo.cnr.it

<sup>3</sup> lferetti@ira.bo.cnr.it

<sup>4</sup> ggiovann@ira.bo.cnr.it

hoc very dense population of mildly relativistic electrons (with a cut-off in the energy distribution at a few MeV) can, in principle, account for the EUV properties.

Atoyan & Völk (2000) have argued that the EUV can be accounted for by IC scattering of the CMB photons from a relic electron population with a radiative cut-off at  $\gamma \geq 500$ , injected in the ICM at the epoch of starburst activity and recently slightly re-energized.

Sarazin (1999; 2000) has pointed out that clusters of galaxies can contain a large number of relic relativistic electrons (with  $\gamma < 300$ ) injected in the past which can account for the EUV excess via IC scattering of CMB photons.

In a recent paper Brunetti et al.(2000) have shown that the radio spectral steepening observed in the case of Coma C (Giovannini et al. 1993; Deiss et al. 1997) may imply the presence of diffuse reacceleration in the cluster volume and the spectrum of a relic population would be stretched toward higher energies thus reducing the emitted EUV flux.

Following the original proposal of Brunetti et al.(1999), in this paper we investigate the possibility that a substantial fraction, if not all, of the EUV excess emission from the Coma cluster can be accounted for by the IC scattering of the CMB photons due to relativistic electrons recently injected in the central part of the cluster by AGN activity and reaccelerated by moderate turbulence in the ICM.

In Sections 2.1 and 2.2 we illustrate the proposed scenario and in Section 2.3 we discuss the possibility that NGC 4869 may supply the required number of relativistic particles; a general discussion is given in Section 3. In Appendix A we calculate the time evolution of the energy distribution of relativistic electrons continuously injected and reaccelerated in the ICM, while relevant formulae used to calculate the synchrotron and IC emitted spectra are given in the Appendix B.

$H_0 = 50 \text{ km s}^{-1} \text{ Mpc}^{-1}$  is assumed throughout.

## 2 Modelling the EUV excess in the Coma cluster

### 2.1 *The proposed scenario*

We assume the scenario of the *two phase* model (Brunetti et al. 2000) in which relic relativistic electrons, continuously injected in the cluster volume in the past, have been recently reaccelerated by diffuse shocks/turbulence probably

induced by a cluster merger. These electrons (the main electron population, *MeP*) are responsible for both the diffuse radio emission and at least for a large fraction of the hard X-rays emitted by Coma via the IC scattering of the CMB photons. The resulting IC spectrum is however flat and falls well below the observed EUV flux.

As already stated in the Introduction, the brightness profile of the EUV excess is much narrower than the radio profile (Bowyer et al. 1999 and references therein) so that, an IC origin of the EUV excess should involve an additional electron population (*AeP*). The requirement is that the synchrotron radio contribution from the *AeP* should be considerably smaller than that from the *MeP* ( $\leq 20 - 30\%$ ), i.e. the energy distribution of the *AeP* should be considerably steeper than that of the *MeP*.

In order to preserve a relatively steep energy distribution during a reacceleration phase it is necessary that the injection of the *AeP* has started recently, i.e. not more than  $\sim 3$  times the reacceleration time. The problem, in this case, is that an efficient injector of relativistic electrons is required to match the energetics necessary to account for the measured EUV. Although the main consequences of this scenario do not depend on the details of the injection, we examine and propose that it can be identified with the recent activity of relatively powerful radio loud AGNs, such as the head tail radio source NGC 4869.

In order to test this hypothesis, in the next Section we model the time-evolution of the *AeP* energy distribution injected in a turbulent ICM.

## 2.2 The model

We consider a simplified model based on the following assumptions:

a) the *AeP* is uniformly injected in the cluster core (spherical geometry) at a constant rate for a time interval  $\Delta t_{inj}$  and with an energy spectrum, typical of the radio galaxies, of the form:

$$Q_{inj}(\gamma) = K_e \gamma^{-\delta} \left( 1 - \frac{\gamma}{\gamma_b^{rg}} \right)^{\delta-2} \quad (1)$$

where  $\gamma$  is the electron Lorentz factor,  $\gamma_b^{rg}$  the break energy and  $\delta > 2$ ;

b) following Sarazin (1999) the electrons lose their energy by synchrotron and Compton losses, the last being dominant because of the relative weakness of the cluster magnetic fields, and at low energies by Coulomb losses, whereas

they are continuously reaccelerated by systematic Fermi processes ( $d\gamma/dt \propto \gamma$ ).

The evolution of the reaccelerated relativistic particles changes depending on whether or not  $\gamma_b^{rg}$  is larger than the asymptotic break energy  $\gamma_b(\infty)$  resulting from the balance between energy losses and gains in the ICM. The time evolution of the  $AeP$  energy spectra are represented in Fig.1 and Fig.2 for these two relevant cases and for values of the parameters representative of the astrophysical problem being discussed (the detailed derivation of the formulae is given in the Appendix A). Fig.1 illustrates the case of  $\gamma_b^{rg} > \gamma_b(\infty)$ . With increasing  $\Delta t_{inj}$  an increasing number of electrons is accumulated below  $\gamma_b(\infty)$ , the spectrum flattens at lower energies due to combined reacceleration and Coulomb losses, while at higher energies (but  $\ll \gamma_b^{rg}$ ) it is  $\propto \gamma^{-\delta+1}$  as in the standard case of continuous injection.

Fig.2 shows the case in which  $\gamma_b^{rg} < \gamma_b(\infty)$ ; again the electron spectrum flattens with increasing  $\Delta t_{inj}$ , but a sharp cut-off is maintained at  $\gamma \leq \gamma_b(\infty)$ .

We have then applied standard formulae (Appendix B) to compute the IC and synchrotron emissions from a spherical volume of 15 arcmin radius (about the extension of EUV excess) by adopting the physical parameters consistent with the two phase model of Brunetti et al.(2000) for Coma. These are: a magnetic field of average strength  $0.5 - 0.6\mu G$  (within  $\sim 15$  arcmin), an acceleration parameter  $\chi = 3.5 \cdot 10^{-16} s^{-1}$  and a Coulomb loss coefficient  $\xi = 1.3 \cdot 10^{-15} s^{-1}$ . With these values  $\gamma_b(\infty) \simeq 1.8 \cdot 10^4$  and electrons of this energy would typically emit synchrotron radiation at a frequency  $\nu \sim 100$  MHz. In the framework of the present model there are then two consequences which follow from the requirement that the predicted radio emission should have a steep spectrum in order not to significantly contribute to the 327–1400 MHz radio spectrum of the Coma cluster: first, the injection period  $\Delta t_{inj}$  cannot be larger than  $\sim 0.3$  Gyr and, second,  $\gamma_b^{rg}$  must be significantly smaller than  $\gamma_b(\infty)$  (Fig. 1 and 2).

By assuming  $\delta = 2.6$ , typical of radio galaxies, and  $\gamma_b^{rg} = 1000$  we have normalized the electron spectrum by requiring that the IC scattering with the CMB photons matches the observed EUV excess and computed the IC and synchrotron emissivities as shown in Fig. 3 and 4.

It is seen that the model accounts for the EUV flux without introducing any significant contribution to the IC X-ray flux derived by Brunetti et al.(2000) model, whose parameters have been adopted here, but the predicted synchrotron emission at low radio frequencies may be significant and may account for the apparent upturn of the radio spectrum indicated by the measurements at low frequencies. If the 74 MHz flux is significantly contributed by the additional electron population (the case  $\Delta t_{inj} = 0.3$  Gyr in Fig.4) the 74–327 MHz

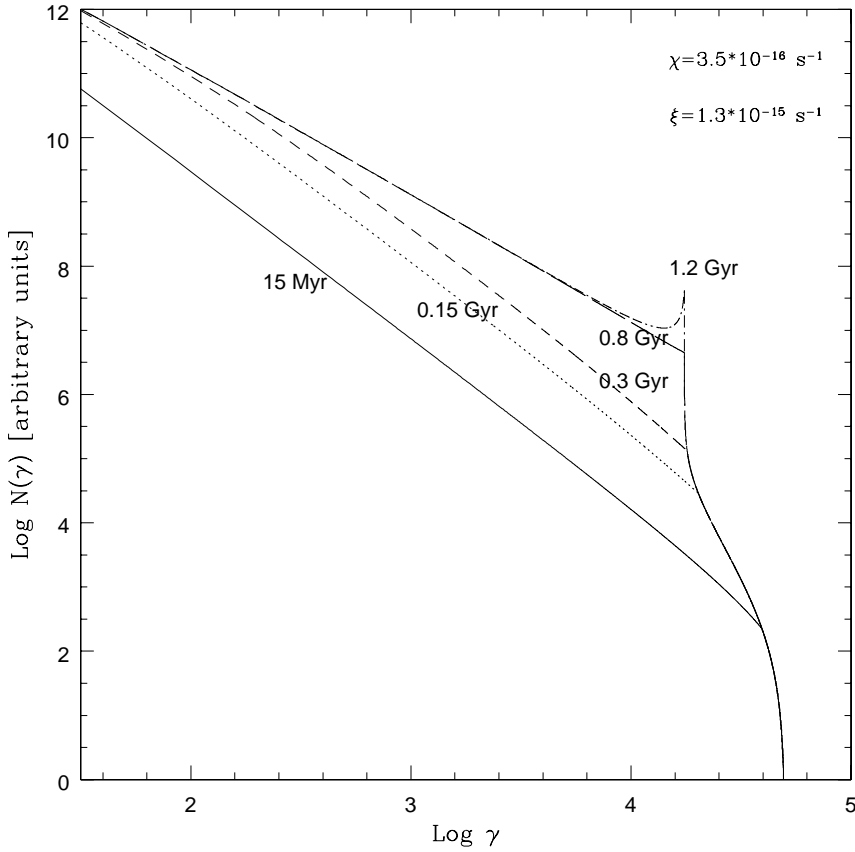


Fig. 1. The energy distribution of electrons injected in the ICM and reaccelerated is reported in arbitrary units. For each curve the injection/reacceleration period  $\Delta t_{inj}$  is given in the panel. The assumed coefficients of reacceleration and of Coulomb losses are  $\chi = 3.5 \cdot 10^{-16} \text{ s}^{-1}$  and  $\xi = 1.3 \cdot 10^{-15} \text{ s}^{-1}$ , respectively; the other parameters are  $B = 0.5 \mu\text{G}$ ,  $\gamma_b^{rg} = 50000$  and  $\delta = 2.6$ .

synchrotron spectrum within  $\sim 15$  arcmin should be steeper ( $\alpha \geq 1$ ) than that between 327–1400 MHz; detailed VLA observations at 74 MHz would help in testing this.

It should also be noticed that in the model the values of  $\gamma_b^{rg}$  and  $\Delta t_{inj}$  are (roughly) inversely correlated: for instance, the adoption of a somewhat higher value for  $\gamma_b^{rg}$ , e.g. 2000, would still be consistent with the low frequency radio data by simply reverting to a smaller value of  $\Delta t_{inj}$ .

### 2.3 NGC 4869 and the EUV excess in Coma

In this Section we compare the energetics of the electron population required by the model to match the EUV excess via IC scattering of CMB photons by the electron population continuously released in the ICM by the AGNs in

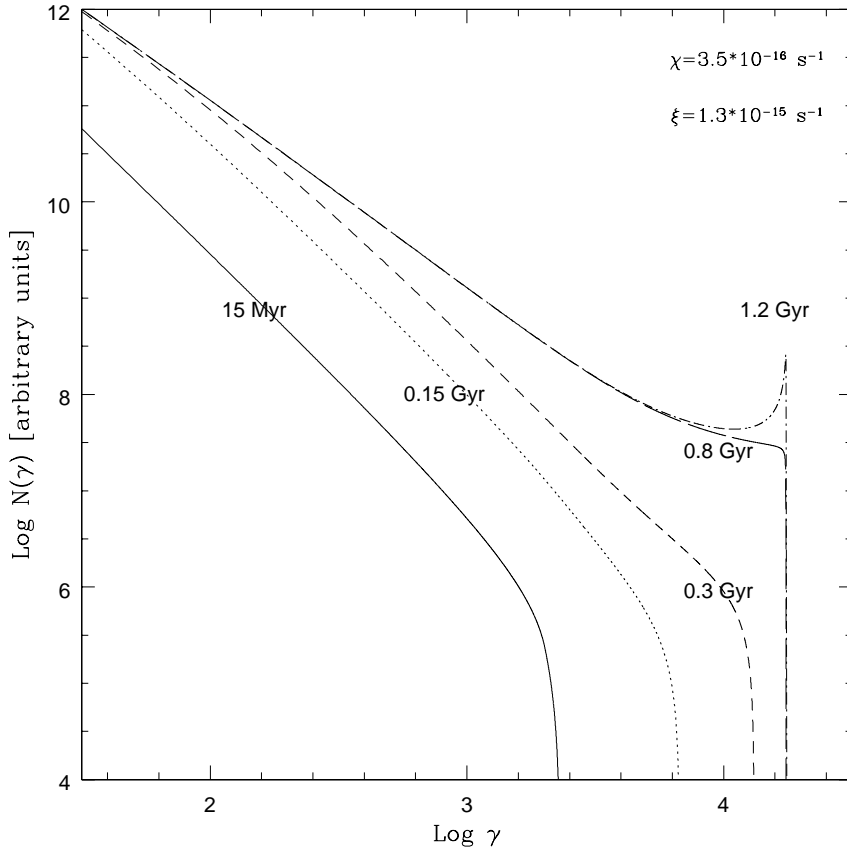


Fig. 2. The calculated electron energy distribution of electrons continuously reaccelerated and injected in the ICM is reported in arbitrary units. In this case the break energy of the injected population,  $\gamma_b^{rg} = 2000$ , is smaller than  $\gamma_b(\infty)$ ; the other parameters being the same of Fig.1.

the Coma cluster. NGC 4869, the head tail radio source, is presently the most powerful radio galaxy in the core of the Coma cluster. The question is whether or not it may supply a sufficient fraction of the energetic electrons required to explain the EUV excess according to the model described in the preceding Section 2.1.

Dallacasa et al.(1989) have reported three frequency (327, 1465, 4885 MHz) spectra of NGC 4869 up to a distance of  $\sim 180$  arcsec from the nucleus and the 327–1465 spectral index up to  $\sim 280$  arcsec.

Feretti et al.(1990) have fitted the synchrotron spectrum of NGC 4869 at different distances from the radio nucleus up to 180 arcsec finding that the break frequency ranges from  $> 50$  GHz close to the nucleus (where the slope of the emitted spectrum is 0.8, i.e.  $\delta = 2.6$ ) to  $< 1$  GHz at larger distances. They interpreted the systematic decrease of the break frequency with distance from the nucleus as due to the ageing of the emitting electrons.

Since we are particularly interested in constraining the electron population at the end of the tail, where electrons are mixed with the ICM, we have fitted the spectral indices of the external part of the tail reported by Dallacasa et al.(1989). We have assumed  $\delta = 2.6$  and a KP model (Kardashev 1962; Pacholczyk 1970) which corresponds to a non re-isotropization of the electron momenta due to the dominance of the synchrotron losses in the tail volume (the SYNAGE fitting software package developed by Murgia & Fanti 1996 has been used). At distances  $> 220$  arcsec the break frequency is not well determined ( $\nu_b \lesssim 200$  MHz) since the 327–1465 MHz spectral index approaches the KP-asymptotic value  $\sim 2$ . By considering the spectral fits and by assuming the particle age to be proportional to the distance from the nucleus (in agreement with Feretti et al. (1990) findings) a break energy  $\gamma_b \lesssim 4000/\sqrt{B_{\mu G}}$  is estimated in the oldest detectable parts of the radio tail ( $\sim 280$  arcsec). It should be stressed that this break energy is only an upper limit to  $\gamma_b^{rg}$  in Eq.(1) since the detected radio flux is emitted by plasma still confined in the radio tail and not yet well mixed with the ICM. We conclude that  $\gamma_b^{rg} \sim 1000$  (given a magnetic field of the radio galaxy  $B \sim 10\mu G$ ; see below), adopted in the model of the preceding Section 2.2, is appropriate to the case of NGC 4869.

Under the simple assumption of an injection rate ( $Q_{inj} = \int Q_{inj}(\gamma)d\gamma$ ) constant with time, the total electron number injected in the cluster volume is  $Q_{inj}\Delta t_{inj}$ . In order to test if NGC 4869 can account for the total number of electrons necessary to match the EUVs, we have calculated  $Q_{inj}$  between 30 and 60 arcsec from the nucleus of the radio galaxy under minimum energy conditions. Since the EUV flux is due to IC by the electrons of the *AeP* with Lorentz factor  $\gamma \sim 300$ , the classical equipartition formulae are not sufficient and we should include low energy electrons in the computation of the minimum energy parameters (Brunetti et al. 1997). By assuming a low energy cut-off in the injected electron spectrum  $\gamma_{min} = 50$  (below which Coulomb losses in the tail would flatten the electron distribution), a ratio = 1 between proton and electron energies and a filling factor = 1, we obtain an equipartition magnetic field in the radio galaxy  $B_{eq} \sim 14.5\mu G$  at a projected distance between 30 and 60 arcsec (20–40 kpc) from the nucleus. The corresponding radiative age  $\sim 4.5 \cdot 10^6$ yr, combined with the synchrotron brightness in the same region (corrected for the steepening of the spectrum), gives  $Q_{inj} \sim 6.5 \cdot 10^{54}$ el yr $^{-1}$ .

By normalizing Eq.1 to this value, we find that the IC contribution to the observed EUV flux from the *AeP* injected in the ICM is  $\sim 30\%$  and  $\sim 40\%$  for  $\Delta t_{inj} = 0.2$  and  $0.3$  Gyr, respectively. Although this time could be long if compared with the typical age of the radio galaxies, we point out that it is similar to the ages estimated in the case of some head tail radio galaxies (e.g. IC 310 and 3C 129, Feretti et al. 1998) and in the case of giant radio galaxies (e.g. B 0313+683, Schoenmakers et al. 1998; B 0319-454, Saripalli, Subrahmanyam, Hunstead 1994).



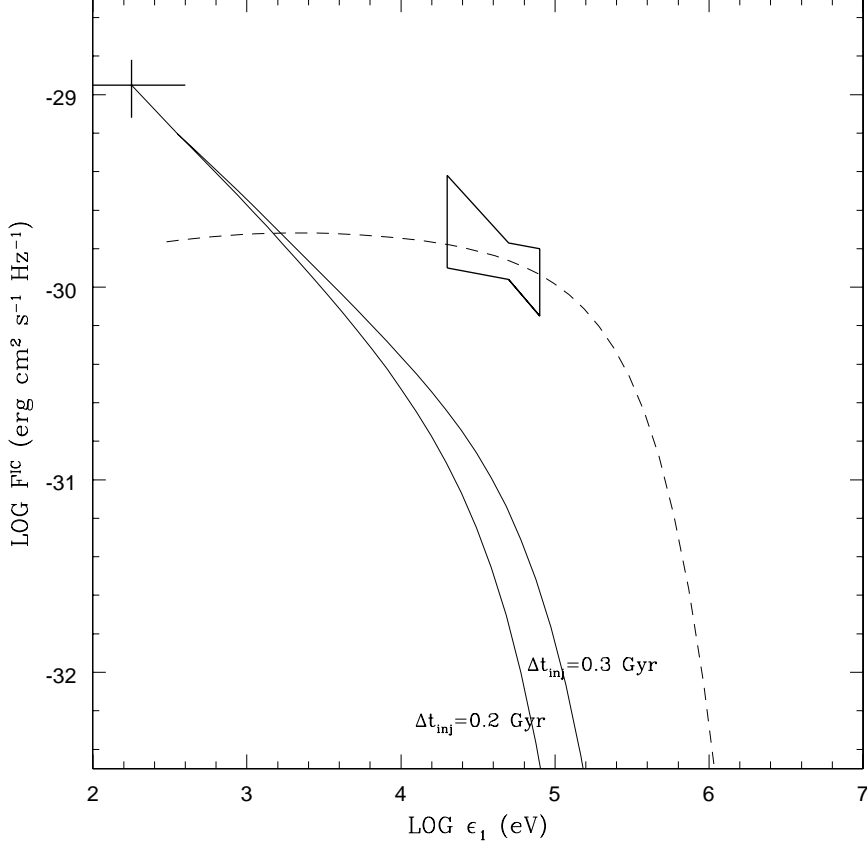


Fig. 3. The calculated IC spectrum from the  $AeP$  injected in the ICM medium is reported for  $\Delta t_{inj} = 0.2$  and  $0.3$  Gyr (solid lines). The curves are normalized to the flux of the EUV excess. In the calculation we have assumed  $\gamma_b^{rg} = 1000$ ,  $\delta = 2.6$  and  $\chi = 3.5 \cdot 10^{-16} \text{s}^{-1}$ . The expected IC contribution from the  $MeP$  in the framework of the *two phase* model (dashed line) is taken by Brunetti et al.(2000).

There is no firm evidence so far of a perfect energy equipartition between magnetic fields and relativistic particles in the radio galaxies, thus we have also investigated the consequences of a moderate departure from equipartition. By assuming a magnetic field strength lower than the equipartition value both the number density of the relativistic electrons and the radiative age increase, thus  $Q_{inj}$  does not critically depend on the departure from the equipartition condition. Specifically we obtain :

$$\frac{Q_{inj}(B)}{Q_{inj}(B_{eq})} = \left(\frac{B_{eq}}{B}\right)^{\frac{\delta+2}{2}} \frac{\left[1 + \left(\frac{B}{B_{IC}}\right)^2\right]}{\left[1 + \left(\frac{B_{eq}}{B_{IC}}\right)^2\right]} \quad (2)$$

where  $B_{IC} \sim 3\mu\text{G}$  is the equivalent field of the CMB. Eq.(2) is reported in Fig.5 : a net increase of  $Q_{inj}$  requires a magnetic field  $B < 0.2 B_{eq}$ . In order to match the EUV flux a magnetic field strength  $B \sim 1/3 - 1/4 B_{eq}$  is required.

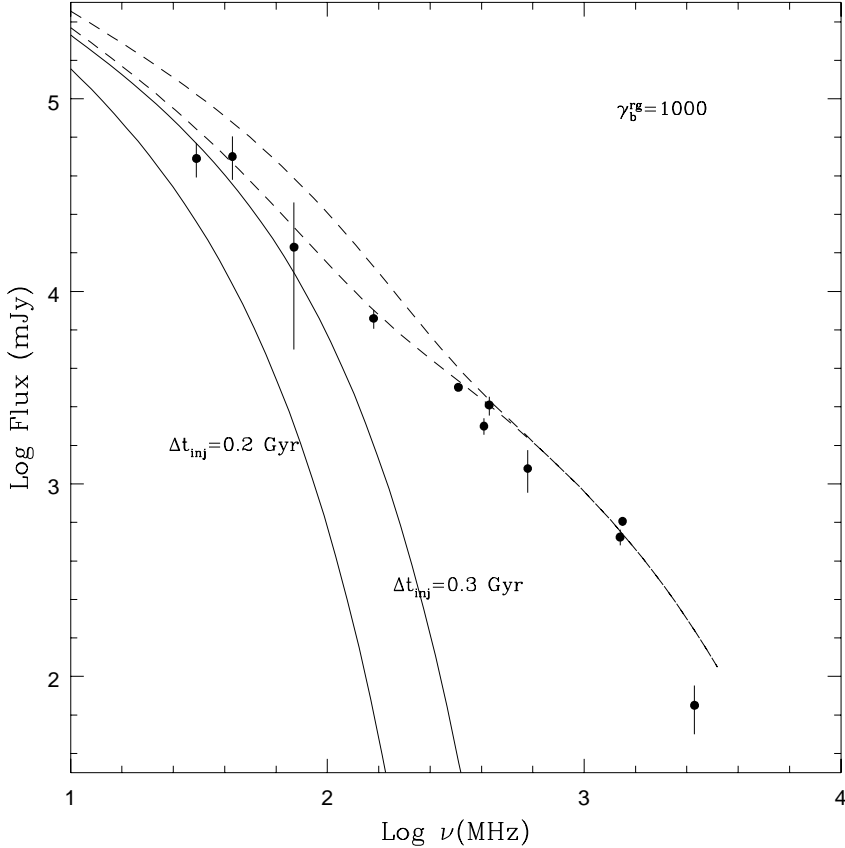


Fig. 4. The calculated synchrotron spectra from the *AeP* injected in the ICM (solid lines) are reported for the IC models represented in Fig.3. A volume averaged  $B = 0.6\mu G$  is assumed. The dashed lines represent the total synchrotron spectrum from Coma C, i.e. the sum of the contributions from the *AeP* and from the reaccelerated relic particles of the *two phase* model (taken from Brunetti et al. 2000).

Implications on the pressure equilibrium between the tailed radio source and the ICM can finally be obtained. By making use of standard equipartition equations, Feretti et al. (1990) have shown that NGC 4869 is in apparent imbalance with the external thermal pressure by a factor  $\sim 10-15$  in the region between 30–60 arcsec and by a larger factor with increasing distance from the nucleus; this imbalance is partly reduced by considering the contribution of the low energy electrons. We have calculated the expected pressure inside the radio volume under our assumptions. The equipartition pressure at 30–60 arcsec from the nucleus is  $\simeq 10^{-11}\text{dyne cm}^{-2}$ , while it is  $\simeq 4 \cdot 10^{-12}\text{dyne cm}^{-2}$  with standard formulae.

Out of equipartition (for an ordered magnetic field) the pressure can be ob-

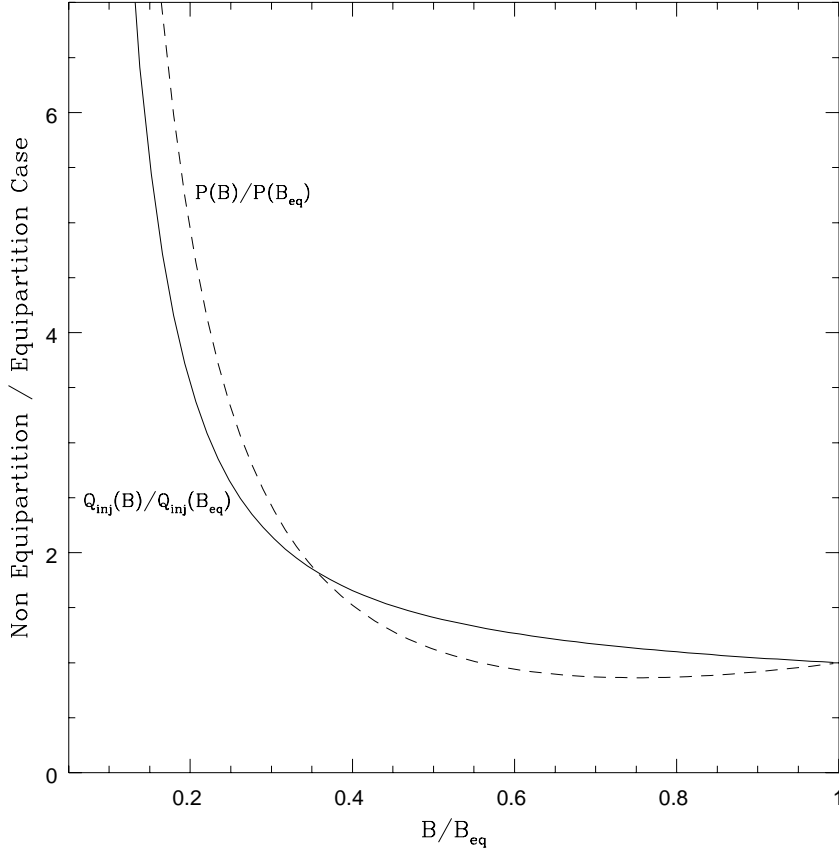


Fig. 5. The particle injection rate (solid line) and the internal pressure (dashed line) normalized to the corresponding values under equipartition conditions are reported for  $\gamma_{min} = 50$  and  $\delta = 2.6$  ( $B < B_{eq}$ ).

tained from Brunetti et al. (1997) equations; one has :

$$\frac{P(B)}{P(B_{eq})} = \frac{3\delta + 3}{3\delta + 7} \left( \frac{B}{B_{eq}} \right)^2 \left( 1 + \frac{1}{3} \frac{4}{\delta + 1} \left( \frac{B_{eq}}{B} \right)^{\frac{\delta+5}{2}} \right) \quad (3)$$

which is reported in Fig.5. Since under our hypothesis the particles contribute to the pressure for only 1/3 of their energy, a moderate departure from equipartition causes a slight decrease of the pressure, which however, rapidly increases for larger departures.

By assuming the magnetic field in NGC 4869 required to match the EUV excess via IC scattering, the internal pressure increases up to  $\sim 2 - 2.5 \cdot 10^{-11} \text{dyne cm}^{-2}$  which is rather close (but a factor  $\sim 2 - 2.5$  below) to the thermal pressure.

### 3 Discussion and Conclusions

It has been previously shown (Brunetti et al 2000) that the radio (synchrotron) and hard X-rays (IC on the CMB photons) properties of Coma C may be explained by a two phase model in which diffuse relic electrons have been efficiently reaccelerated throughout the cluster volume for a period of  $\sim 1$  Gyr by the turbulence and associated Fermi type mechanisms excited in the ICM by a recent merger (main electron population, *MeP*).

By adopting this model we have shown here that a steady injection in the cluster core of an additional fresh population of relativistic electrons (Fig.6) may explain the EUV excess, recently determined by Bowyer et al.(1999), as IC scattering of the CMB photons. Detailed computations of the time evolution of the injected electron spectrum show that internal consistency within the complete model requires a relatively steep injection spectral index ( $\delta \sim 2.6$ ), however typical of the radio galaxies, and an injection starting time  $\leq 0.3$  Gyr, in which case there is no significant contribution to the synchrotron emission in the 327-1400 MHz band and to the total X-ray flux. Nevertheless, it should be pointed out that an important contribution to the emission at low radio frequencies ( $\leq 100$  MHz; Fig.4) may be present, so that improved measurements at long radio wavelengths may provide a test of the proposed interpretation of the EUV excess and, of course, constrain the model parameters.

The luminosity of the EUV excess is  $\sim 1.5 \cdot 10^{42}$  erg/sec. An IC origin with the spectral shape of our model needs a total number of injected electrons  $\sim 4 \cdot 10^{63}$ . We have explored the possibility that a large fraction of these electrons may have been injected by the powerful head tail radio galaxy NGC 4869 orbiting in the cluster core. By assuming that NGC 4869 has been constantly active in the past 0.3 Gyr (an age comparable to that of a number of giant and head tail radio galaxies) we find, based on minimum energy conditions in the tail, that about 40% of the required number of electrons may have been released to the ICM; a full complement is achieved with a moderate departure from the equipartition resulting in a magnetic field intensity about a factor  $\sim 3$  weaker. The total energy of the electrons deposited in the ICM is  $\sim 4 \cdot 10^{59}$  erg which is not unreasonable for a radio galaxy.

We stress that, although the internal pressure is considerably increased with respect to previous estimates based on classical equipartition formulae, the radio tail is still well confined by the hot ICM: the pressure gap is reduced by almost an order of magnitude, but the tail is still underpressurized by a factor 2–3. The introduction of a filling factor and of a relativistic proton component may now easily bring to a pressure equilibrium.

In Fig.7 the observed EUV radial profile is compared with that predicted by our model based on the simple assumption of a spherical and uniform distribution of the relativistic particles centered on the cluster centre. It is seen that the model provides a very good fit of the data at an angular distance  $> 3$  arcmin from the centre which includes  $\sim 90 - 95\%$  of the EUV excess. We note that in the innermost 3 arcmin the radial profile samples a region containing the cD galaxy NGC 4874 so that an additional contribution to the EUV flux may be expected. Furthermore, it should be stressed that at smaller radii the azimuthal distribution of the EUV excess is very sensitive to small scale brightness/temperature fluctuations of the hot ICM. If the relativistic electrons are mainly supplied by NGC 4869 then the EUV brightness distribution should be related to some extent with the orbital path followed by the tailed radio source. At present the tail's end is positioned at an angular distance of  $\sim 6$  arcmin from the cluster centre, so that a shift between the X-ray and EUV maxima may be expected. However, most of the injected relativistic plasma could have been stirred around the cluster core in the available time scale by the turbulence generated by the random motion of the galaxies; this may have considerably smoothed out the distribution of the relativistic particles on the cluster core size and thus that of the emitted EUV photons. Detailed mapping of the EUV excess would obviously be of great importance.

We point out that our model, although specifically developed for the Coma cluster, may have a wider application predicting the existence of sizeable fluxes of excess EUV photons from galaxy clusters where large numbers of relativistic electrons are injected in the cluster cores by powerful AGN activity, or other energetic events such as a minor merger, during a reacceleration phase. However, due to the requirement of a contemporaneous presence of efficient Fermi type turbulence reacceleration and of an efficient recent injection of relativistic electrons in the cluster core (i.e. the presence of powerful AGNs), we claim that in the clusters with radio haloes a non-thermal EUV excess due to the proposed scenario would be more rare than the hard X-ray excess.

Finally, if a relic population of relativistic electrons is commonly associated with clusters of galaxies (Sarazin 1999), the related EUV excess from IC scattering of CMB photons is expected to be more common in clusters without radio halo than in those with radio halo where diffuse reacceleration processes may stretch toward higher energies the electron spectrum.

## Acknowledgements

We are grateful to S. Bowyer and T. Ensslin for useful discussions and suggestions. This work was partly supported by the Italian Ministry for University and Research (MURST) under grant Cofin98-02-32.

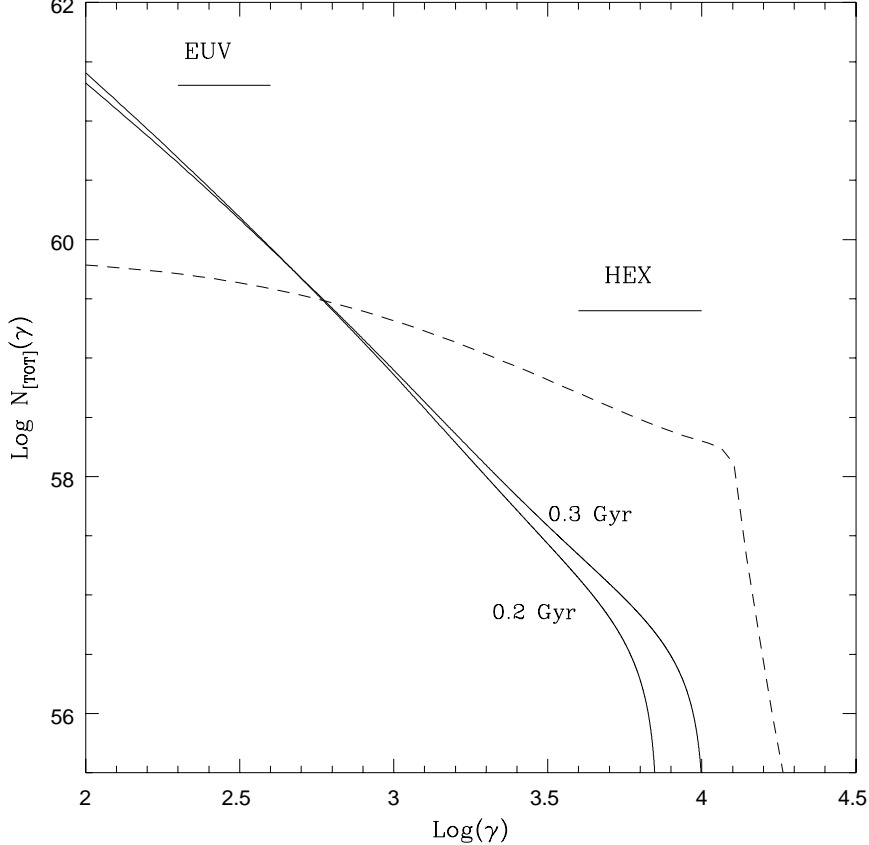


Fig. 6. The energy distribution integrated over the cluster volume of the main electron population (dashed line) and of the additional electron population (solid lines) are shown in arbitrary units. The typical energies of the electron emitting via IC in the hard X-ray band (HEX) and in the EUV band are also showed.

### A Appendix A: Time evolution of injected and reaccelerated electrons

The time evolution of the particle energy distribution  $N(\gamma, t)$  is obtained by solving the kinetic equation (e.g. Kardashev 1962):

$$\frac{\partial N(\gamma, t)}{\partial t} = -\frac{\partial}{\partial \gamma} \left[ \frac{d\gamma}{dt} N(\gamma, t) \right] + Q_{inj}(\gamma, t) \quad (\text{A.1})$$

where  $\gamma$  is the Lorentz factor. We assume an injection function  $Q_{inj}(\gamma)$  typical of the radio galaxies (Eq.1).

Once injected, the electrons lose energy via Coulomb and radiation losses and are reaccelerated by Fermi processes (here assumed to be systematic :

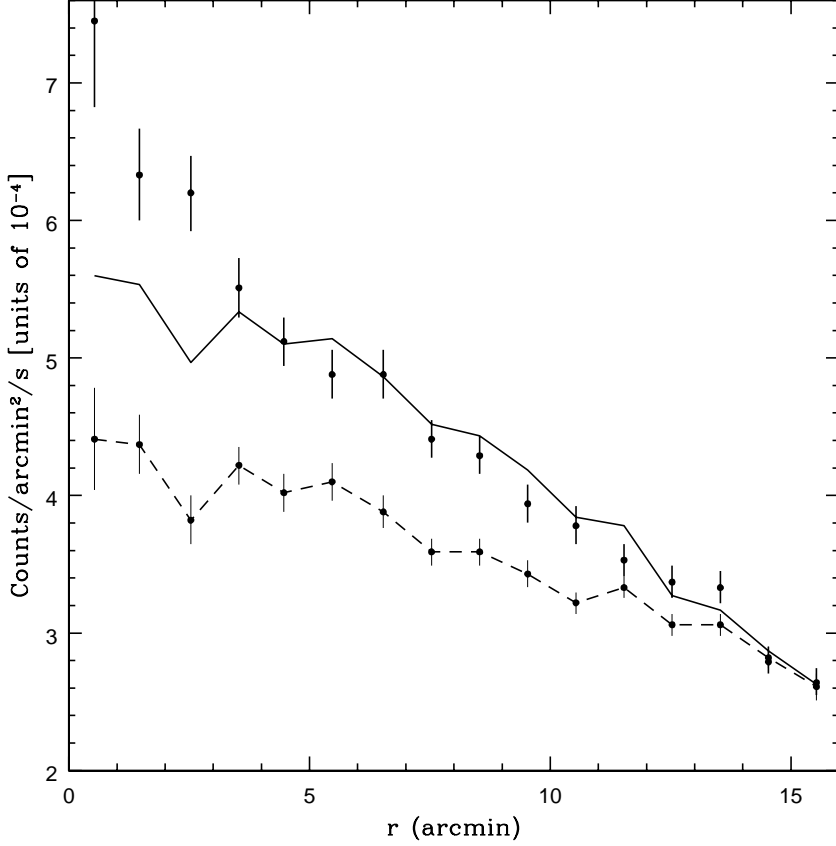


Fig. 7. The comparison between the model calculations and the observed EUV profile is reported. The model EUV profile (solid line) is obtained by taking into account the instrumental background plus the expected EUV from the X-ray plasma (dashed line). The data for the instrumental background and EUV from X-ray plasma and observed EUV excess (bold data points) are taken from Bowyer et al. (1999).

$d\gamma/dt = \chi\gamma$ ), thus, the evolution of the energy of the electrons is :

$$\frac{d\gamma}{dt} = \chi\gamma - \xi - \beta\gamma^2 \quad (\text{A.2})$$

where  $\chi$  is the reacceleration efficiency,  $\xi$  the coefficient of the Coulomb losses :

$$\xi \simeq 1.2 \cdot 10^{-12} n \left( 1 + \frac{\ln(\gamma/n)}{75} \right) \sim 1.4 \cdot 10^{-12} n \quad (\text{A.3})$$

and  $\beta$  that of the radiative losses :

$$\beta(z) = 1.9 \cdot 10^{-9} \left( \frac{2}{3} B^2 + B_{IC}^2(z) \right) \quad (\text{A.4})$$

$B_{IC}(z)$  being the equivalent magnetic field strength of the CMB. Under these assumptions the time evolution of the energy of the electrons is :

$$\gamma(\tau) = \frac{\gamma(t_i)(\sqrt{q}/\tanh(x) + \chi) - 2\xi}{2\beta\gamma(t_i) + \sqrt{q}/\tanh(x) - \chi} \quad (\text{A.5})$$

with  $t_i$  the time at which the injection has started,  $q = \chi^2 - 4\xi\beta > 0$ ,  $x = \frac{\sqrt{q}}{2}\tau$  and  $\tau$  the time interval since the injection.

The time-evolution of the spectrum injected in the unit time interval is obtained by solving the kinetic equation with  $Q_{inj} = 0$ . We obtain :

$$N(\gamma, \tau) = K_{\epsilon} q \frac{(1 - \tanh(x))^2}{(2\beta\gamma_b \tanh(x))^2} \left(1 - \frac{\gamma}{\gamma_b(\tau)}\right)^{\delta-2} \cdot \gamma^{-\delta} \{1 + S[\gamma; \gamma_b(\tau)]\}^{-\delta} \left(1 - \frac{\gamma}{\gamma_b^{rg}} \frac{1 + S[\gamma; \gamma_b(\tau)]}{1 - \gamma/\gamma_b(\tau)}\right)^{\delta-2} \quad (\text{A.6})$$

where

$$S[\gamma; \gamma_b(\tau)] = \frac{\xi\gamma^{-1} - \chi}{\beta\gamma_b(\tau)} \quad (\text{A.7})$$

and the break energy at time  $\tau$  is:

$$\gamma_b(\tau) = \frac{1}{2\beta} \left\{ \frac{\sqrt{q}}{\tanh(x)} + \chi \right\} \xrightarrow{\tau \rightarrow \infty} \frac{\sqrt{q} + \chi}{2\beta} \equiv \gamma_b(\infty) \quad (\text{A.8})$$

The solution of Eq.(A.1) after an injection and reacceleration period  $\Delta t_{inj}$  is then obtained by integrating Eq.(A.6) over the injection time. However, for a given Lorentz factor  $\gamma$ , only the contributions of the injected electrons with a maximum energy larger than  $\gamma$  should be considered. In order to do this we introduce the largest energy of the electron population with  $\tau = \Delta t_{inj}$  (i.e. the oldest one); from Eq.(A.5), with  $\gamma(t_i) = \gamma_b^{rg}$ , one has :

$$\gamma_{max} = \frac{\gamma_b(\Delta t_{inj}) - \xi/(\beta\gamma_b^{rg})}{1 + [\gamma_b(\Delta t_{inj}) - \chi/\beta](\gamma_b^{rg})^{-1}} \begin{cases} \xrightarrow{\gamma_b^{rg} \rightarrow \infty} \gamma_b(\Delta t_{inj}) \\ \xrightarrow{\gamma_b^{rg} = \gamma_b(\infty)} \gamma_b(\infty) \end{cases} \quad (\text{A.9})$$

The integration is performed as follows (Fig A1):



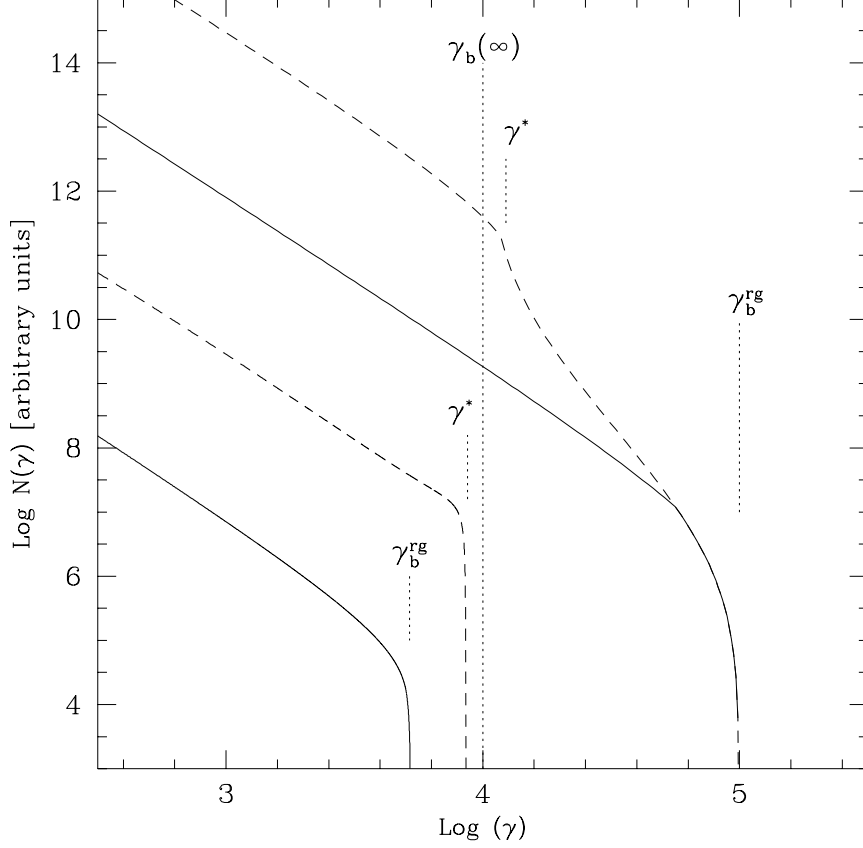


Fig. A.1. Sketch of the electron spectrum evolution. In the picture the asymptotic break energy is  $\gamma_b(\infty) = 10^4$ . The injected spectra (solid lines) and those calculated after an injection time  $\Delta t_{inj}$  (dashed lines) are given both in the case  $\gamma_b^{rg} > \gamma_b(\infty)$  and  $\gamma_b^{rg} < \gamma_b(\infty)$ . The number of electrons, in arbitrary units, has a different normalization for the two cases.

- case  $\gamma_b^{rg} > \gamma_b(\infty)$  :

$$N(\gamma, \Delta t_{inj}) = \int_0^{\mathcal{T}} N(\gamma, \tau) d\tau \quad (\text{A.10})$$

where  $\mathcal{T} = \Delta t_{inj}$  for  $\gamma < \gamma_{max}$ , while

$$\mathcal{T} = \frac{1}{\sqrt{q}} \ln \left( \frac{\chi - \sqrt{q} - 2\beta\mathcal{F}(\gamma)}{\chi + \sqrt{q} - 2\beta\mathcal{F}(\gamma)} \right) \quad (\text{A.11})$$

for  $\gamma > \gamma_{max}$ , where the function

$$\mathcal{F}(\gamma) = \frac{\gamma\gamma_b^{rg}}{\gamma_b^{rg} - \gamma} \{1 + S[\gamma; \gamma_b^{rg}]\} \xrightarrow{\gamma_b^{rg} \rightarrow \infty} \gamma \quad (\text{A.12})$$

- case  $\gamma_b^{rg} < \gamma_b(\infty)$  :

$$N(\gamma, \Delta t_{inj}) = \int_{\mathcal{T}}^{\Delta t_{inj}} N(\gamma, \tau) d\tau \quad (\text{A.13})$$

where  $\mathcal{T} = 0$  for  $\gamma < \gamma_b^{rg}$ , while it is given by Eq.(A.11) for  $\gamma > \gamma_b^{rg}$ .

In the calculations we have not considered the effect of statistical Fermi acceleration; this would further complicate the equations. In this case the main effect of the electron diffusion in the momentum space is a smoothing of the calculated features of the energy distribution. In particular the energy cut off at  $\gamma_{max}$  would become an exponential decrease. However, the synchrotron and IC emitted spectrum are not sensitive to minor differences in the energy distribution being given by the convolution with the synchrotron and IC Kernel functions, respectively. As a consequence, the systematic Fermi approach is adequate to the aim of this paper.

## B Appendix B: Synchrotron and IC formulae used in the model computations

In order to calculate the synchrotron emission by the *AeP* we have assumed a magnetic field smoothly varying in space and tangled on a scale significantly smaller than the variation scale of its intensity. This allows us to consider the emitted synchrotron spectrum isotropic. In this case the synchrotron emissivity is obtained by integrating the isotropic synchrotron Kernel over the electron energy and angular distribution (cf. Westfold 1959; Pacholczyk 1970). The synchrotron emissivity per unit solid angle is:

$$j^S \left( \frac{\nu}{\nu_b}, \Delta t_{inj} \right) = \frac{\sqrt{3}}{8\pi} \frac{e^3}{mc^2} \frac{K_e B}{w^{\delta-1}} \frac{q}{\beta^2} \int_0^{\frac{\pi}{2}} d\theta \sin^2 \theta \int_0^1 du F \left( \frac{\nu/\nu_b}{u^2 \sin \theta} \right) u^{-\delta} \int_0^{\mathcal{T}(u)} d\tau \{1 + S(u, \tau)\}^{-\delta} \left( 1 - u \frac{w}{\gamma_b^{rg}} \frac{1 + S(u, \tau)}{1 - uw/\gamma_b(\tau)} \right)^{\delta-2} \gamma_b^{-2}(\tau) \left( 1 - \frac{1}{\tanh(x)} \right)^2 \left( 1 - u \frac{w}{\gamma_b(\tau)} \right)^{\delta-2} \quad (\text{B.1})$$

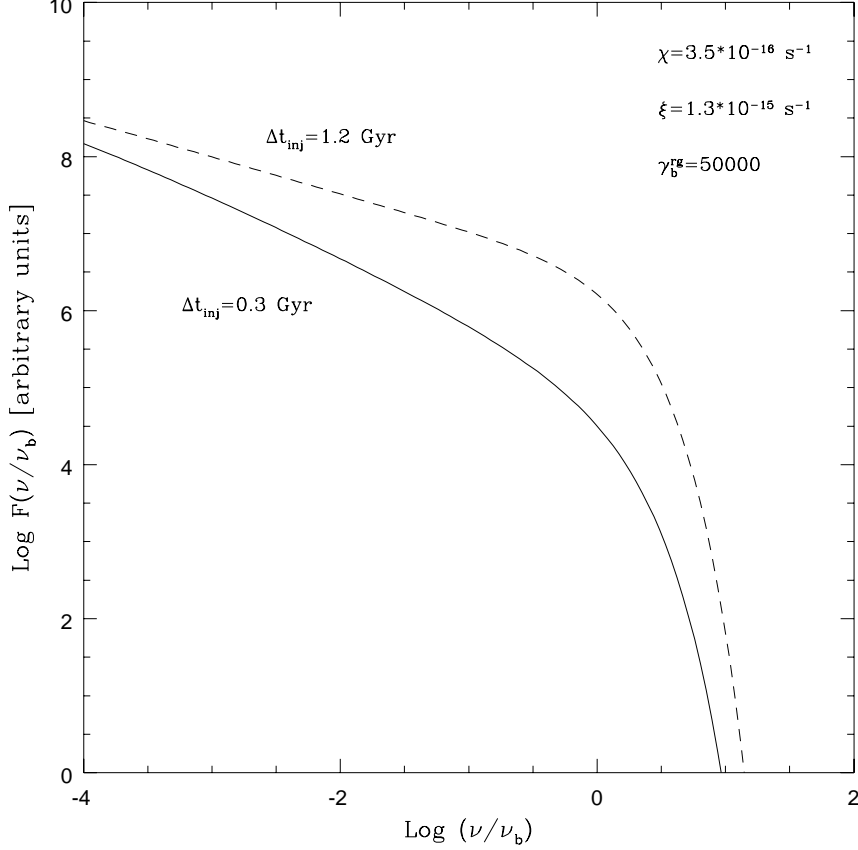


Fig. B.1. The calculated synchrotron spectrum from electrons continuously reaccelerated and injected in the ICM medium is reported for different injection period  $\Delta t_{inj}$  as given in the panel. The calculation is performed for  $\chi = 3.5 \cdot 10^{-16} \text{s}^{-1}$ ,  $\xi = 1.3 \cdot 10^{-15} \text{s}^{-1}$ ,  $\gamma_b^{rg} = 50000$  and  $\delta = 2.6$ .

where

$$S(u, \tau) = \frac{\xi u^{-1} w^{-1} - \chi}{\beta \gamma_b(\tau)} \quad (\text{B.2})$$

$u = \gamma/w$ ,  $w = \gamma_b^{rg}$  or  $\gamma_b(\Delta t_{inj})$  if  $\gamma_b^{rg} > \gamma_b(\infty)$  or  $\gamma_b^{rg} < \gamma_b(\infty)$ , respectively,  $F$  is the isotropic electron Kernel (e.g. Pacholczyk 1970) and the other quantities are defined in Appendix A.

Because of the angular distribution of the CMB photons is isotropic, the IC spectrum is obtained by integrating the electron energy distribution of the  $AeP$  over the isotropic IC Kernel in the ultrarelativistic case (e.g. Blumenthal & Gould 1970). The assumptions for the magnetic field distribution adopted in the case of the synchrotron spectrum, guarantee the isotropy of the IC emission even if the effect of synchrotron losses are important for the electron energy distribution. The IC emissivity per unit solid angle is given by:

$$\begin{aligned}
j^{IC}(\epsilon_1, \Delta t_{inj}) = & K_e \frac{2^{\delta+3} r_0^2 \pi}{c^2 h^2} \frac{q}{\beta^2} \int \frac{(\epsilon/\epsilon_1)^{\frac{\delta+5}{2}} d\epsilon}{\exp\{\epsilon/kT_{cmb}\} - 1} \\
& \int_1^{y_{max}} dy y^{\frac{\delta+1}{2}} \left(1 - 2y + 2\ln y + \frac{1}{y}\right) \\
& \int_0^{\tau(\gamma)} d\tau \{1 + S(y, \tau)\}^{-\delta} \\
& \left\{ \left(1 - \frac{y}{y_b(\tau)}\right) \left(1 - \frac{y}{y_b^{rg}} \frac{1 + S(y, \tau)}{1 - y/y_b(\tau)}\right) \right\}^{\delta-2} \\
& y_b(\tau) \left(1 - \frac{1}{\tanh(x)}\right)^2
\end{aligned} \tag{B.3}$$

where

$$S(y, \tau) = \frac{\xi y^{-1} (y_b^{rg})^{-1} - \chi}{\beta y_b(\tau)} \tag{B.4}$$

while,  $y_b^{rg} = (\epsilon_1/4\epsilon)(\gamma_b^{rg})^{-2}$ ,  $y_{max} = (\epsilon_1/4\epsilon)w^{-2}$ , and  $y_b(\tau) = (\epsilon_1/4\epsilon)(\gamma_b(\tau))^{-2}$ .

An example of the synchrotron spectrum obtained from Eq.(B.1) is given in Fig.B1. Here, the break frequency is defined as the critical synchrotron frequency of the electrons with the maximum Lorentz factor (in this case  $\gamma_b^{rg}$ ) and pitch angle  $\theta=90^\circ$ . Following the evolution of the electron energy distribution (e.g. Figs. 1 & 2) the synchrotron spectrum flattens with increasing  $\Delta t_{inj}$ .

## References

- Arabadjis J.S., Bregman J.N., 1999, *Apj* 514, 607
- Atoyan A.M., Völk H.J., 2000, in press; astro-ph/9912557
- Berghöfer T.W., Bowyer S., Korpela E., 2000, *ApJ* 535, 615
- Blumenthal G.R., Gould R.J., 1970 *Rev. of Mod. Phys.* 42, 237
- Bonamente M., Lieu R., Mittaz J.P.D., 2000, *ApJ L* in press; astro-ph/0011186

- Bowyer S., Lampton M., Lieu R., 1996, *Science* 274, 1338
- Bowyer S., Berghöfer T.W., 1998, *ApJ* 506, 502
- Bowyer S., Berghöfer T.W., Korpela E., 1999, *ApJ* 526, 592
- Brunetti G., Setti G., Comastri A., 1997, *A&A* 325, 898
- Brunetti G., Feretti L., Giovannini G., Setti G., 1999 in *Diffuse Thermal and Relativistic Plasma in Galaxy Clusters*, eds. H.Böhringer, L.Feretti, P.Schuecker, MPE Report 271, p.263
- Brunetti G., Setti G., Feretti L., Giovannini G., 2000, *MNRAS* in press; astro-ph/0008518
- Donnelly R.H., Markevitch M., Forman W., Jones C., Churazov E., Gilfanov M., 1999, *ApJ* 513, 690
- Ensslin T.A., Biermann P.L., Kronberg P.P., Wu X.-P., 1997, *ApJ* 477, 560
- Ensslin T.A., Lieu R., Biermann P.L., 1999, *A&A* 344, 409 1978, *A&A* 69, 253
- Dallacasa D., Feretti L., Giovannini G., Venturi T., 1989, *A&AS* 79, 391
- Feretti L., Dallacasa D., Giovannini G., Venturi T., 1990, *A&A* 232, 337
- Feretti L., Dallacasa D., Giovannini G., Tagliani A., 1995, *A&A* 302, 680
- Feretti L., Giovannini G., 1996, *IAUS* 175, 347
- Feretti L., Giovannini G., Klein U., et al., 1998, *A&A* 331, 475
- Fusco-Femiano R., Dal Fiume D., Feretti L., et al., 1999 *ApJ* 513, 197L
- Giovannini G., Feretti L., Venturi T., Kim K.T., Kronberg P.P., 1993, *ApJ* 406, 399
- Giovannini G., Tordi M., Feretti L., 1999, *NewA* 4, 141.

- Kardashev N.S., 1962, *Sov. Ast.* 6, 317
- Lieu R., Mittaz J.P.D., Bowyer S., et al., 1996, *Science* 274, 1335
- Lieu R., Mittaz J.P.D., Bowyer S., et al., 1996, *ApJ* 458, L5
- Lieu R., Ip W.-H., Axford W.I., Bonamente M., 1999, *ApJ* 510, L25
- Lieu R., Bonamente M., Mittaz J.P.D., 2000, *A&A*, in press; astro-ph/0010610
- Murgia M, Fanti R., 1996, *IRA internal report*, 228/96
- Pacholczyk A.G., 1970, *Radio Astrophysics*, eds. G. Burbidge & M. Burbidge, Freeman and Company, San Francisco
- Sarazin C.L., 1999, *ApJ* 520, 529
- Sarazin C.L., 2000, in *Large Scale Structure in the X-ray Universe*, p.81, eds. M.Plionis, I. Georgantopoulos
- Sarazin C.L., Lieu R., 1998, *ApJL* 494, 177
- Saripalli L., Subrahmanyan R., Hunstead R.W., 1994, *MNRAS* 269, 37
- Schoenmakers A.P., Mack K.-H., Lara L., et al., 1998, *A&A* 336, 455
- Völk H.J., Atoyan A.M., 1999, *APh* 11, 73